https://doi.org/10.5194/egusphere-2026-2644
Preprint. Discussion started: 20 May 2026

Methane in the Asian Monsoon Anticyclone and global UTLS behavior observed in ACE-FTS satellite data

You Yi[1], William J. Randel[2], Laura L. Pan[2], Yi Liu[3], Shuangxi Fang[1], Zhaonan Cai[3], Teresa Campos[2], Benjamin Gaubert[2]

[1]Zhejiang Carbon Neutral Innovation Institute, ZheJiang University of Technology, HangZhou, ZheJiang, China
[2]NSF National Center for Atmospheric Research, Boulder, CO, USA
[3]State Key Laboratory of Atmospheric Environment and Extreme Meteorology, Institute of Atmospheric Physics, Chinese Academy of Sciences, Beijing, China

Correspondence to: You Yi (yiyou@zjut.edu.cn)

Abstract. Methane in the upper troposphere and lower stratosphere (UTLS) plays a critical role in atmospheric composition and radiative forcing, yet the processes governing its vertical structure and variability remain insufficiently understood. Here, we use high-quality satellite observations from the Atmospheric Chemistry Experiment Fourier Transform Spectrometer (ACE-FTS), together with in situ measurements, to characterize the vertical structure and global seasonal behavior of methane in the UTLS, with particular emphasis on the role of Asian Summer Monsoon (ASM). Methane exhibits a relative maximum that peaks near the tropopause inside the ASM anticyclone. The largest relative enhancement—defined as the difference between air inside and outside the anticyclone—occurs above the tropopause and extends poleward to the north. This behavior contrasts sharply with carbon monoxide, which is confined within the anticyclone. The seasonal cycle of methane near the tropical tropopause reaches a maximum in boreal autumn, following the summer peak in surface fluxes and deep convection. This phase lag reflects the combined effects of ASM transport and subsequent large-scale redistribution following the breakdown of the anticyclone. The enhanced methane signal propagates upward into the lower stratosphere, consistent with the upwelling branch of the Brewer–Dobson circulation (BDC). Beyond the seasonal cycle, ACE-FTS data show a pronounced hemispheric asymmetry in lower stratospheric methane trends, consistent with previously reported changes in other long-lived trace constituents. Together, these results provide new observational evidence that ASM transport imprints a distinct methane structure above the tropopause and plays a key role in shaping UTLS variability on a global scale.

1 Introduction

Methane (CH_4) is the second most important anthropogenic greenhouse gas after carbon dioxide. Its atmospheric lifetime of approximately 9-10 years allows methane to be transported over large distances and to influence both tropospheric and stratospheric composition. Understanding the global budget of methane therefore requires careful examination not only of surface sources and sinks, but also of the vertical redistribution processes that connect the lower atmosphere with the upper troposphere and lower stratosphere (UTLS) (Patra et al. 2011; Zeng et al., 2021; Saunois et al., 2025; Fu and Dong, 2026).

https://doi.org/10.5194/egusphere-2026-2644
Preprint. Discussion started: 20 May 2026

The ASM exerts a particularly strong influence on UTLS composition (e.g. Randel et al., 2010). Intense deep convection over South Asia and East Asia can loft boundary air masses, rich in methane and other pollutants, to the upper troposphere within several days (Randel et al., 2006; Baker et al., 2012; Pan et al., 2016, 2024). The upper tropospheric anticyclone acts as a quasi-closed reservoir in the UTLS, trapping these enhancements for weeks to months (Park et al., 2007; Vogel et al., 2014). Through subsequent transport by the Brewer-Dobson circulation (BDC), these regional emissions can have consequences for the global stratospheric composition budget (Ploeger et al., 2013; 2017; Vogel et al., 2019; Riese et al, 2025). However, despite extensive studies on ASM transport, the global distribution of methane in the UTLS and its linkage to ASM transport remain poorly quantified, particularly above the tropopause and beyond the anticyclone region.

Methane in the UTLS is especially important for climate forcing. Enhancements near the tropopause strengthen the greenhouse effect, while subsequent oxidation in the stratosphere produces additional water vapor that alters radiative balance and modulates ozone photochemistry (Riese et al., 2012; Fleming et al., 2015). These processes highlight methane in the UTLS as a sensitive driver of short-term climate feedback.

The Atmospheric Chemistry Experiment Fourier Transform Spectrometer (ACE-FTS) provides high-quality vertical profiles of CH_4 from the upper troposphere to the stratosphere, with near-global coverage and a long, continuous record since 2004 that captures seasonal cycles, interannual variability, and long-term trends. These observations are particularly valuable for examining methane behavior in the UTLS and for placing regional transport signals into a global context.

In this study, we first assess the quality of ACE-FTS observations in the ASM region using high vertical-resolution in-situ measurements from balloon and aircraft that extend into the lower stratosphere. Subsequently, we contrast the observed behavior of CH_4 with that of carbon monoxide (CO), which is a tracer of combustion with a shorter photochemical lifetime of ~1 month, also measured by ACE-FTS and widely used to diagnose UTLS transport associated with the ASM anticyclone. We then assess the behavior of CH_4 in the global UTLS and characterize the global seasonal cycle and long-term trends. Together, these analyses provide new observational evidence for the role of ASM transport in shaping the distribution and seasonal variability of CH_4 in UTLS on a global scale.

2 Data and Methods

2.1 ACE-FTS measurements of CH_4 and CO

The Atmospheric Chemistry Experiment–Fourier Transform Spectrometer (ACE-FTS), onboard the Canadian SCISAT satellite launched in 2003, is a high-resolution infrared Michelson spectrometer (0.02 cm^{-1}) that measures solar occultation transmission spectra between 2.2–13.3 μm (Bernath et al., 2005). From these spectra, vertical profiles of trace gases are retrieved with a typical vertical resolution of 3–4 km spanning from about 5 km to 75 km altitude. Due to its orbit geometry, ACE-FTS provides ~30 occultations per day with latitude coverage that shifts seasonally, yielding tropical observations primarily for four months each year (February, April, August, and October, e.g. Randel et al., 2012). Methane is retrieved on an oversampled 1 km grid with effective resolution ~3 km, and its profiles have been extensively validated. Comparisons with Halogen Occultation Experiment (HALOE) satellite data show

https://doi.org/10.5194/egusphere-2026-2644
Preprint. Discussion started: 20 May 2026

differences of ~5 % below 35 km and ~10–15 % at 40–60 km (De Mazière et al., 2008), while intercomparisons with Michelson Interferometer for Passive Atmospheric Sounding (MIPAS) and balloon data suggest a small negative bias (of order –10 %) in the upper troposphere–lower stratosphere. For ACE-FTS CO, the precision and accuracy are 0.66×10^3ppt and less than 2%, respectively (Schmidt et al., 2024). Overall, ACE-FTS CH_4 and CO retrievals are considered robust for UTLS studies when standard quality flags are applied, and they provide a unique multi-decadal record for investigating the seasonal cycle and interannual variability of methane.

The V5 retrievals from ACE-FTS measurements spanning 2005-2023 are used in this study. ACE-FTS provides near-global coverage approximately every three months, thus we group the data into four seasons: December-January-February (DJF), March-April-May (MAM), June-July-August (JJA), and September-October-November (SON). For each season and year, we examine all profiles within every 30° latitude bands. A small number of points falling outside three local standard deviation are removed. Climatological concentrations are then constructed by combining all measurements from 2005 to 2023 for each season. The data are gridded onto a $5^o \times 10^o$ latitude-longitude grid using a Gaussian-weighted average of measurements within 500 km of each grid box, following an approach similar to Randel et al. (2012).

2.2 In-situ measurements

2.2.1 AirCore observations

The AirCore observations were conducted in August 2019 and 2020 over the Tibetan Plateau to investigate the role of ASM transport in redistributing greenhouse gases. During the campaign, eight vertical profiles of CO_2, CH_4, and CO were collected using the AirCore technique. The AirCore system consists of a long, thin stainless-steel tube carried aloft by a balloon, which samples the ambient atmosphere during descent from ~25 km to the surface, followed by a laboratory analysis with a Picarro G2401. Further details of the campaign are provided in Yi et al. (2026).

Here, we focus on eight CH_4 and CO profiles to compare with ACE-FTS measurements and to highlight their contrasting structures near the tropopause (Fig. 1). Both species exhibit clear enhancements in the upper troposphere, but with distinct vertical structures: CO decreases rapidly with height beginning about 2 km below the tropopause, whereas CH_4 reaches a maximum near the tropopause before sharply declining. Previous studies show that deep convection uplifts surface pollutants to ~13 km within a week, after which air masses are confined within the anticyclone and ascend slowly over weeks to months (Vogel et al., 2019). During this slow ascent, CO decreases due to its shorter photochemical lifetime, whereas CH_4 remains relatively stable (Yi et al., 2024). Building on these in situ observations, we use ACE-FTS data to examine the large-scale distributions of CH_4 and CO and the role of tropopause-level methane maxima in the global UTLS.

https://doi.org/10.5194/egusphere-2026-2644
Preprint. Discussion started: 20 May 2026

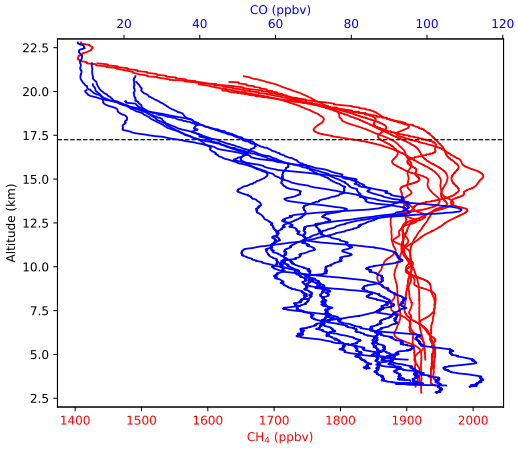

Figure 1: CO (blue) and CH_4 (red) profiles on Tibetan Plateau in August 2019 and 2020 obtained from AirCore. Black dashed line marks the average lapse-rate tropopause.

2.2.1 In situ measurements from the ACCLIP campaign

The Asian summer monsoon Chemical and Climate Impact Project (ACCLIP) was a large-scale aircraft campaign conducted over the western Pacific in August 2022 to investigate the impact of the ASM on atmospheric composition in the UTLS. The campaign deployed two research aircrafts equipped with state-of-the-art instruments capable of measuring numerous chemical species. The NCAR Gulfstream-V (GV) primarily operated below ~ 16 km, while the NASA WB-57 reached altitudes of up to ~ 20 km. We use CH_4 and CO vertical profiles measured by Picarro G2401-mc aboard the NCAR GV and the Whole Air Sampling (WAS) aboard the NASA WB-57 to compare with the ACE-FTS measurements from a broader perspective. The WAS samples were also analyzed by Picarro G2401-mc. For Picarro G2401-mc, CO and CH_4 precision are 5 ppbv and 0.5 ppbv within 1 min, respectively. The accuracy of CO and CH_4 is ± 3 and 5 ± 0.1%, respectively. Note that the ACCLIP campaign targeted highly polluted regions, whereas the spatial resolution of ACE-FTS is insufficient to fully resolve local structures. Additional details about the ACCLIP campaign are provided in Pan et al. (2025).

3 Results

3.1 Comparison of ACE-FTS with in-situ measurements

ACE-FTS measurements in the ASM region are compared with AirCore observations and ACCLIP campaign. For the AirCore comparison, we select ACE-FTS profiles within 33°N-41°N and 80°-110°E, centered around the AirCore observation location (37.8°N, 95.3°E). To increase the sampling size given the sparse satellite coverage over this region, we include measurements covering 4 recent years from August 2019 to 2022, resulting in a total of 8 collocated profiles. For the ACCLIP campaign, ACE-FTS measurements within 20°N-40°N and 120°E-150°E are selected, covering most of the flight tracks. The same 4-year temporal window (August 2019–2022) is used to obtain adequate

https://doi.org/10.5194/egusphere-2026-2644
Preprint. Discussion started: 20 May 2026

regional sampling for ACE-FTS, yielding 19 profiles within this region. For each altitude level, the mean and standard deviation are calculated across all selected profiles.

Comparisons of methane vertical profiles from ACE-FTS, AirCore, and the ACCLIP campaign show overall good agreement (Fig. 2). ACE-FTS captures the broad CH_4 enhancement layer between 12 km and 16 km and the rapid decrease above 17 km, as expected due to oxidation in the stratosphere. Concentrations are systematically lower than those observed during ACCLIP, which preferentially sampled more polluted air masses. We also include CO to provide a contrast to CH_4 under the influence of the ASM anticyclone. The ACE-FTS CO profiles agree well with in-situ measurements, showing the enhancement layer at 13.5–14.5 km followed by a pronounced decrease above, reaching stratospheric background levels at ~19 km.

Overall, ACE-FTS measurements are consistent with the in-situ observations. Both datasets reveal a stronger CH_4 enhancement and a sharper gradient near the tropopause than observed for CO, suggesting that CH_4 is more efficiently transported upward within the ASM anticyclone, while CO is largely confined to lower altitudes due to its shorter lifetime. The long-term high quality satellite measurements provide opportunity to investigate the contrasting large-scale behavior between CH_4 and CO under the influence of ASM transport and to assess their potential impact on the global UTLS.

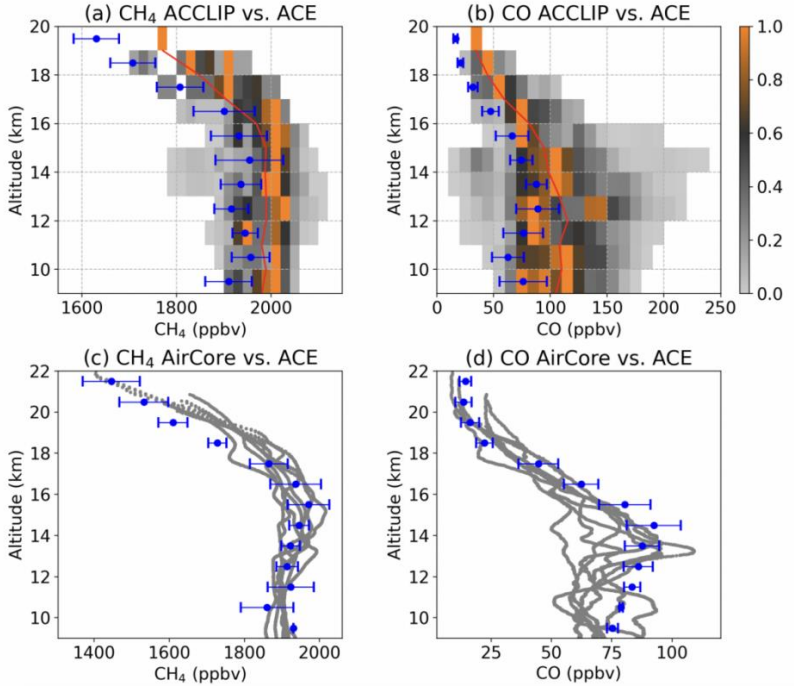

Figure 2: Comparison of ACE-FTS measurements with in-situ data in ASM region. (a) Layer-normalized relative frequency distributions of CH_4 (the horizontal bin size is every 20 ppbv, the vertical bin size is 0.5 km), red line shows the mean CH_4 mixing ratio for each vertical bin level. Measurement of average CH_4 vertical profiles obtained from ACE-FTS (blue dots). Blue error bars indicate one sigma standard deviation of the averages at each level; (b) The same as (a) but for

https://doi.org/10.5194/egusphere-2026-2644
Preprint. Discussion started: 20 May 2026

CO; (c) Gray lines are CH_4 profiles in Fig. 1, blue dots and error bars are the same with (a) but near the location of AirCore campaign; (d) the same as (c) but for CO.

3.2 Contrasting Vertical Structures of CH_4 and CO in the ASM Anticyclone

Near-global climatological distributions of CH_4 and CO in JJA, together with the corresponding climatological stream function indicating the ASM anticyclone, are shown in Fig. 3. The climatological fields are constructed from Gaussian-weighted gridded average of ACE-FTS observations during 2005-2023. With two decades of continuous ACE-FTS observations, the sampling density is sufficiently high at lower latitudes. The gridded results reveal clear enhancements of both CO and CH_4 within the region of the ASM anticyclone, with the horizontal gradient between inside and outside the anticyclone being more pronounced for CO. This feature is consistent with Park et al. (2008), who found that enhancements of tropospheric trace species within the anticyclone are closely linked to their photochemical lifetimes, with shorter-lived species exhibiting the larger increases.

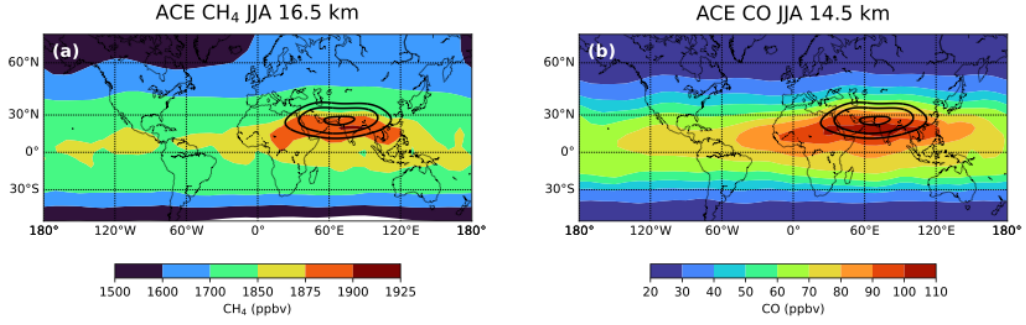

Figure 3: Horizontal distributions of JJA climatological mixing ratios from ACE-FTS data during 2005-2023. (a) CH_4 at 16.5 km and (b) CO at 14.5 km. The black solid contours indicate the ASM anticyclone, defined by the stream function from ERA5 reanalysis at the corresponding altitude.

The climatological vertical structure of CH_4 and CO within the ASM anticyclone, averaged over 20-120°E, is shown in Fig. 4. Both species exhibit enhanced mixing ratios within the anticyclone (10-30°N), but at different altitudes. For CO, the peak mixing ratio occurs around 14 km, approximately 2 km below the tropopause, whereas for CH_4, the highest mixing ratio is found around 16 km, extending across the tropopause. A similar vertical structure of CH_4 within the anticyclone has also been reported by Park et al. (2004). These results highlight the contrasting vertical behavior of trace gases with different photochemical lifetimes: CH_4 persists into the tropopause region, while CO decays more rapidly, producing a sharp decline at lower altitudes, consistent with in situ observations (von Hobe et al., 2021; Yi et al., 2024).

https://doi.org/10.5194/egusphere-2026-2644
Preprint. Discussion started: 20 May 2026

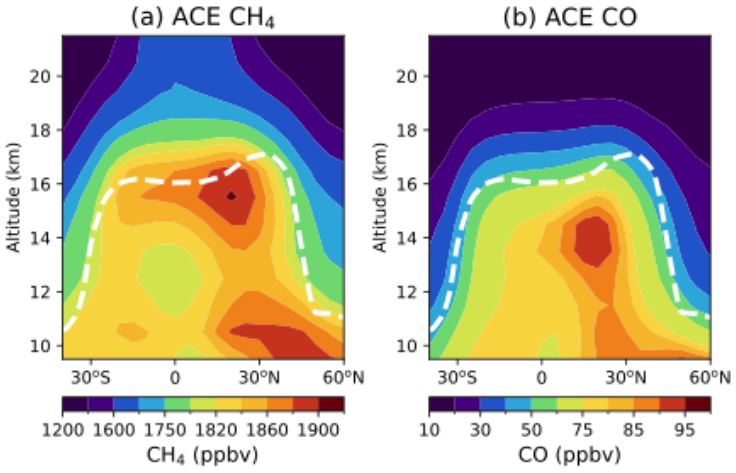

Figure 4: Meridional cross-sections of JJA climatological mixing ratios over the ASM region (20–120°E), derived from the horizontal maps shown in Fig. 3. Observed (a) CH_4 mixing ratios and (b) CO mixing ratios from ACE-FTS. The white dashed lines denote the climatological lapse-rate tropopause from ERA5 reanalysis.

Enhancements of CO and CH_4 inside the anticyclone are further quantified in Fig. 5 by subtracting the profiles outside the anticyclone (longitudes outside of 20-120°E) from those inside (longitudes 20-120°E). The largest CH_4 enhancements occur above the tropopause and extend poleward (north) of the anticyclone, whereas CO enhancements are confined within the anticyclone. The methane enhancement structure suggests that long-lived tracers inside the ASM anticyclone are preferentially transported into the northern extratropical lower stratosphere, likely due to weaker confinement on the northern side of the anticyclone above the westerly jet and the tropopause. This result is consistent with Riese et al. (2025), who reported strongly enhanced methane mixing ratios, but no comparable enhancement in CO, for in-situ measurements of high-latitude air masses influenced by export from the ASM region.

https://doi.org/10.5194/egusphere-2026-2644
Preprint. Discussion started: 20 May 2026

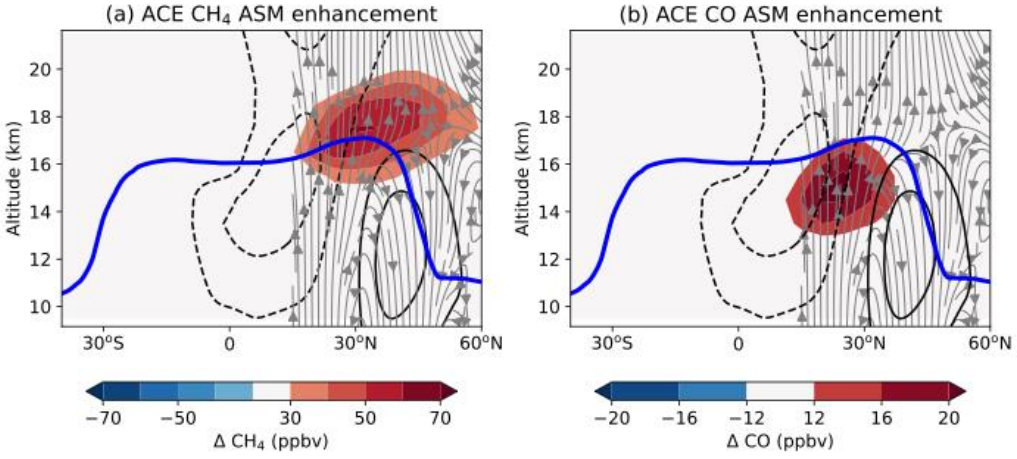

Figure 5: Meridional cross section of the ASM enhancement (averaged over 20-120°E) relative to background (longitudinally averaged except 20-120°E) for (a) CH_4 and (b) CO from ACE-FTS. Blue lines indicate the lapse-rate tropopause. Solid and dashed black lines (10 m/s and 20 m/s) represent westerly and easterly winds over 20-120°E, respectively. Gray streamlines depict the corresponding composites of meridional velocity (m/s) and vertical velocity (mm/s).

3.3 Methane seasonality in the global UTLS

We examine the seasonality of CH_4 near the tropopause as observed by ACE-FTS and relate it to surface flux seasonality, with particular emphasize on the role of ASM transport in shaping CH_4 variability near the tropical tropopause layer (TTL). Understanding CH_4 seasonality in the TTL is critical because this region controls the entry of CH_4 into the stratosphere, where CH_4 is oxidized to form water vapor (Fu and Dong, 2026).

https://doi.org/10.5194/egusphere-2026-2644
Preprint. Discussion started: 20 May 2026

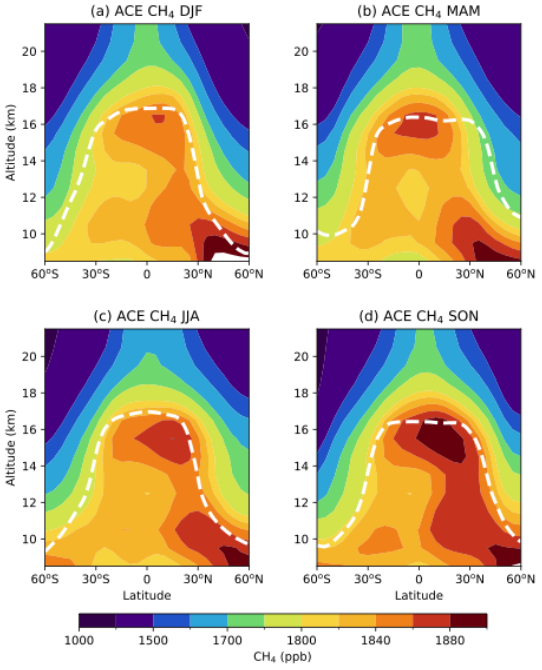

Figure 6: Climatological meridional cross sections of zonal mean CH_4 for the (a) DJF, (b) MAM, (c) JJA and (d) SON seasons derived from ACE-FTS observations, averaged over period 2005-2023. White dashed lines denote the lapse-rate tropopause.

Climatological zonal mean cross sections of CH_4 mixing ratio from ACE-FTS are shown for the four seasons in Fig. 6. Overall behavior shows maximum CH_4 mixing ratios in the northern hemispheric (NH) troposphere, due to natural and anthropogenic sources over the continents (Saunois et al., 2025). Additionally, a relative maximum in CH_4 persists near the tropical tropopause throughout the year, with the highest values observed during the SON season, when it also extends above the tropopause.

The climatological horizontal distribution of the CH_4 annual cycle at 16.5 km is shown in Fig. 7, together with climatological deep convection indicated by low outgoing longwave radiation (white contours). In JJA, CH_4 exhibits a pronounced maximum around the ASM anticyclone. This feature is linked to the deep convection and strong confinement of the anticyclone during ASM (Park et al., 2004; Randel et al., 2006; Pan et al., 2016). The maximum persists into SON and extends throughout the global tropics. During the boreal autumn season, the chemical composition within the anticyclone can be transported into the tropics as the anticyclone breaks up (Vogel et al., 2015; Orbe et al., 2015).

https://doi.org/10.5194/egusphere-2026-2644
Preprint. Discussion started: 20 May 2026

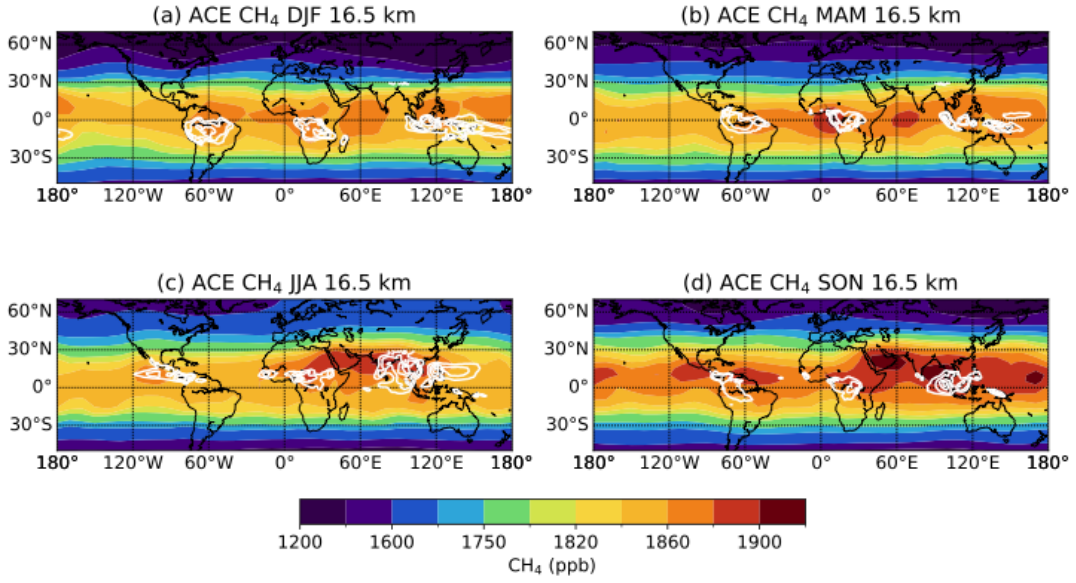

Figure 7: Climatological horizontal distributions of CH_4 at 16.5 km for (a) DJF, (b) MAM, (c) JJA and (d) SON seasons derived from ACE-FTS observations gridded at 5° latitude by 10° longitude, averaged over the period 2005-2023. The white contours represent the region of strongest deep convection, as identified by outgoing longwave radiation (OLR<=220 K).

215

We further examine the role of ASM transport in shaping CH_4 seasonality in the tropics using the seasonal variability of CH_4 surface fluxes and the area of low outgoing longwave radiation (OLR) as a proxy for deep convection over 15°S – 30°N (Fig. 8). CH_4 surface fluxes and deep convection are both strongest during boreal summer, driving the observed systematic increases in upper tropospheric CH_4. The strongest deep convection in boreal summer occurs in
220 the region of the ASM, which is also one of the major summertime methane source regions (Yu et al., 2023). Together with the UTLS anticyclonic circulation, this leads to localized CH_4 maxima (e.g. Fig. 3a). The seasonal break-up of the monsoon, together with convective transport over other longitudes, leads to the global UTLS maximum in the tropics in SON.

https://doi.org/10.5194/egusphere-2026-2644
Preprint. Discussion started: 20 May 2026

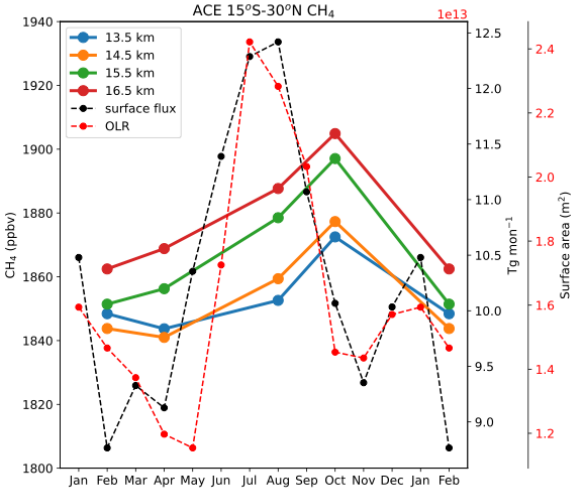

225

Figure 8: Seasonal cycle of ACE-FTS zonal mean CH_4 mixing ratio climatology at 13.5 – 16.5 km averaged over 15°S-30°N (solid lines). Red dashed line indicates the intensity of deep convection to the UTLS, using a proxy of surface area of outgoing longwave radiation less than 220 W/m^2 over 15°S-30°N. Black dashed line shows a climatology of CH_4 surface flux within the latitude band of 15°S-30°N derived from Saunois et al., (2025).

230

The seasonal maximum of CH_4 during SON can be traced upward into the tropical lower stratosphere. Fig. 9 shows the climatological annual cycle of CH_4 seasonal anomalies (subtracting the annual average values at each level) averaged over 20°S-20°N in the UTLS, derived from ACE-FTS observations. Note that ACE-FTS tropical sampling is limited to four months per year (February, April, August, and October). The observations show the boreal autumn
235 positive anomaly extends up to the tropopause, consistent with the seasonal peak shown in Fig. 6. This positive anomaly gradually propagates upward into the lower stratosphere, reflecting the climatological tropical upwelling branch of the Brewer-Dobson circulation (as indicated by the white dashed line in Fig. 9, with a slope of ~ 8 km/year). In addition, the relative minimum of CH_4 above the tropopause during boreal summer is consistent with seasonally weak tropical upwelling.

https://doi.org/10.5194/egusphere-2026-2644
Preprint. Discussion started: 20 May 2026

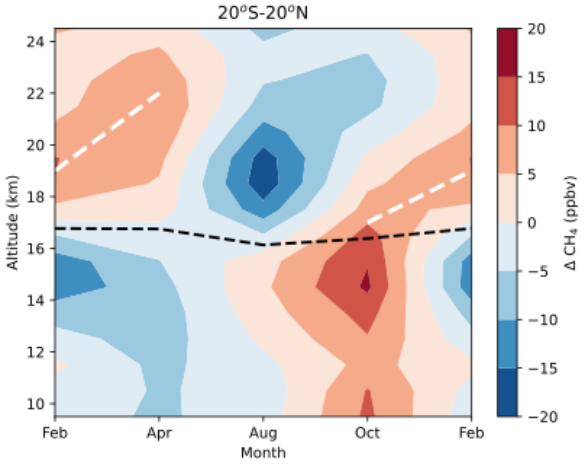

Figure 9: Climatological annual cycle of zonal-mean CH_4 seasonal anomalies in the UTLS, averaged over 20°S-20°N, based on ACE-FTS observations for the period 2005-2023. The black dashed lines denote the WMO tropopause obtained from ERA5 reanalysis. The sloping white dashed line highlights the upward propagation of the maximum positive CH_4 anomaly originating near the tropopause, with a speed of ~8 km/year.

3.4 CH_4 trends

Global increases in tropospheric CH_4 over recent decades are well-known and increasing trends in upper tropospheric CH_4 over the past decades have been previously reported from ACE-FTS measurements (Schmidt et al., 2024). Time series of seasonal ACE-FTS data in the tropical UTLS (15°S – 30°N; Fig. 10a) highlight increases over time, along with the repeating seasonal maximum during boreal summer and autumn. Linear trends in these data are estimated using the Long-term Ozone Trends and Uncertainties in the Stratosphere (LOTUS) multivariate regression code (SPARC, 2019). Results in Fig. 10b show broad positive trends of +3-4%/decade in the global troposphere, with a slight relative maximum near the tropical tropopause (which is not statistically significant). In contrast, CH_4 trends in the lower stratosphere (above 18 km) show a pronounced hemispheric asymmetry, with near-zero trends in the Northern Hemisphere (NH) and positive trends in the Southern Hemisphere (SH). This pattern is consistent with trends after 2000 for other long-lived stratospheric tracers (e.g. Han et al., 2019; Strahan et al., 2020; Prignon et al., 2021; Dube et al., 2023, 2025) and with reanalysis-driven simulations indicating relative aging of air in the NH compared to the SH (Ploeger and Garny, 2022).These results suggest low-frequency structural changes in the BDC, characterized by a strengthened and upward-shifted deep branch and a weakened shallow branch in the NH relative to the SH, as a likely cause of these systematic changes.

https://doi.org/10.5194/egusphere-2026-2644
Preprint. Discussion started: 20 May 2026

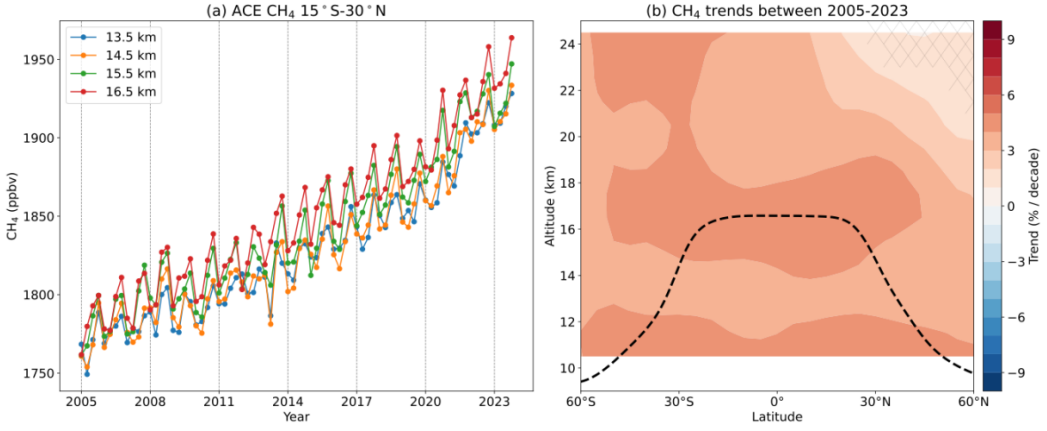

Figure 10: (a) Time series of zonal mean CH_4 mixing ratio averaged over 15ºS-30ºN for multiple levels, as obtained from ACE-FTS (colored solid line). (b) CH_4 trends in UTLS over the period January 2005-December 2023, as calculated by LOTUS regression code (SPARC, 2019). Hatched regions are insignificant at the 2σ level. Black dashed line represents the WMO-tropopause obtained from ERA5 reanalysis.

4 Summary and discussion

This study investigates methane variability associated with ASM transport and its impact on the global UTLS using high-quality ACE-FTS observations. Comparisons against high vertical-resolution AirCore profiles and aircraft measurements demonstrate that ACE-FTS captures both the upper-tropospheric CH_4 enhancement and the sharp vertical gradients near the tropopause. Consistent agreement is found for ACE-FTS CO, further supporting the robustness of the ACE-FTS observations. Both ACE-FTS observations and in-situ measurements reveal CH_4 and CO enhancements within the anticyclone, with distinct vertical structures: CH_4 maximum extends up to the local tropopause, whereas CO decreases sharply about 2 km below it. This highlights distinct transport characteristics of the short- and long-lived tracers associated with the ASM.

The contrast in tracers between the interior and exterior of the anticyclone reveals distinct spatial structures for CH_4 and CO: the largest CH_4 enhancements occur poleward to the north and above the tropopause, whereas the strongest CO enhancements are found below the tropopause within the anticyclone. The behavior demonstrates that air masses inside the ASM anticyclone are preferentially transported into the northern extratropical lower stratosphere (i.e. Ploeger et al., 2013), likely due to weaker confinement on the northern side of the anticyclone above the westerly jet and the tropopause.

On a global scale, an upper tropospheric CH_4 maximum is observed throughout the year in the tropics, maximizing during boreal summer (JJA) and autumn (SON). This climatological maximum likely arises as a result of enhanced deep convection overlying maximum surface CH_4 fluxes during boreal summer (Fig. 8). The ASM circulation is part of this boreal summer maximum, and the confining ASM circulation further enhances CH_4 in the monsoon region (e.g. Fig. 3a). As the ASM anticyclone dissipates in boreal autumn, this CH_4 maximum broadens toward the tropics, and mixing ratios near the tropical tropopause layer reach their seasonal maximum. The seasonal peak further

https://doi.org/10.5194/egusphere-2026-2644
Preprint. Discussion started: 20 May 2026

propagates upward into the lower stratosphere at the climatological ascent rate of approximate 8 km yr-1, associated with the upwelling branch of Brewer-Dobson circulation (Fig. 9).

ACE-FTS data show the well-known growth in CH_4 over time, with increases of 3-4%/decade throughout the troposphere and UTLS region. A clear hemispheric asymmetry is evident in lower stratospheric trends (above 18 km), with negative values in the NH and positive values in the SH. The spatial pattern is consistent with post-2000 trends in other long-lived tracers reported in recent studies, suggesting a weakened shallow branch of the BDC in the NH relative to the SH during these years (Ploeger and Garny, 2022). But these asymmetric stratospheric CH_4 trends have little impact on the ASM or global tropical tropopause region.

Overall, these results highlight the role of the ASM in shaping methane variability in the UTLS and its subsequent influence on global distributions. As emphasized in the Introduction, understanding the redistribution processes that couple the lower atmosphere with the UTLS is important for constraining the global methane budget and evaluating its radiative impacts. The long-record high-quality ACE-FTS methane data provides a unique benchmark for testing model performance and for quantifying the ASM's role in CH_4 transport and variability.

Data availability

The AirCore data can be accessed through https://doi.org/10. 57760/sciencedb.09463. The ACE-FTS satellite data can be accessed through https://databace.scisat.ca. The ACCLIP data can be accessed through https://data.eol.ucar.edu/master_lists/generated/acclip/.

Author contributions

WR and YY designed the study; YY and WR performed the data analysis; YY and WR wrote the manuscript. YL, SF, ZC, and YY conducted the AirCore campaign in China. LP and TC conducted the ACCLIP methane and carbon monoxide measurements over the western Pacific; BG provided additional insights on the draft. All authors contribute to the revision of the manuscript.

Competing interests

The contact author has declared that none of the authors has any competing interests.

Acknowledgments

We thank the ACE-FTS team for providing the observation data and European Center for Medium-Range Weather Forecasts for providing the ERA5 data product.

Financial support

This work was supported by the Jing-Jin-Ji Regional Integrated Environmental Improvement-National Science and Technology Major Project of Ministry of Ecology and Environment of China (No. 2025ZD1200701). The National

https://doi.org/10.5194/egusphere-2026-2644
Preprint. Discussion started: 20 May 2026

Center for Atmospheric Research is supported by the US National Science Foundation. This work was partially supported under NASA Grant 80NSSC20K0928.

References

Baker, A. K., Schuck, T. J., Brenninkmeijer, C. A. M., Rauthe-Schöch, A., Slemr, F., Velthoven, P. F. J., and Lelieveld, J.: Estimating the contribution of monsoon-related biogenic production to methane emissions from South Asia using CARIBIC observations, Geophys. Res. Lett., 39, 813–819, https://doi.org/10.1029/2012gl051756, 2012.

Bernath, P. F., McElroy, C. T., Abrams, M. C., Boone, C. D., Butler, M., Camy-Peyret, C., Carleer, M., Clerbaux, C., Coheur, P. -F., Colin, R., DeCola, P., DeMazière, M., Drummond, J. R., Dufour, D., Evans, W. F. J., Fast, H., Fussen, D., Gilbert, K., Jennings, D. E., Llewellyn, E. J., Lowe, R. P., Mahieu, E., McConnell, J. C., McHugh, M., McLeod, S. D., Michaud, R., Midwinter, C., Nassar, R., Nichitiu, F., Nowlan, C., Rinsland, C. P., Rochon, Y. J., Rowlands, N., Semeniuk, K., Simon, P., Skelton, R., Sloan, J. J., Soucy, M. -A., Strong, K., Tremblay, P., Turnbull, D., Walker, K. A., Walkty, I., Wardle, D. A., Wehrle, V., Zander, R., and Zou, J.: Atmospheric Chemistry Experiment (ACE): Mission overview, Geophys. Res. Lett., 32, https://doi.org/10.1029/2005gl022386, 2005.

Climate Change 2021 – The Physical Science Basis, https://doi.org/10.1017/9781009157896, 2023.

Dubé, K., Tegtmeier, S., Bourassa, A., Zawada, D., Degenstein, D., Sheese, P. E., Walker, K. A., and Randel, W.: N2O as a regression proxy for dynamical variability in stratospheric trace gas trends, Atmos. Chem. Phys., 23, 13283–13300, https://doi.org/10.5194/acp-23-13283-2023, 2023.

Dubé, K., Tegtmeier, S., Ploeger, F., and Walker, K. A.: Hemispheric asymmetry in recent stratospheric age of air changes, Atmos. Chem. Phys., 25, 1433–1447, https://doi.org/10.5194/acp-25-1433-2025, 2024.

East, J. D., Jacob, D. J., Balasus, N., Bloom, A. A., Bruhwiler, L., Chen, Z., Kaplan, J. O., Mickley, L. J., Mooring, T. A., Penn, E., Poulter, B., Sulprizio, M. P., Worden, J. R., Yantosca, R. M., and Zhang, Z.: Interpreting the Seasonality of Atmospheric Methane, Geophys. Res. Lett., 51, 494–505, https://doi.org/10.1029/2024gl108494, 2024.

Fleming, E. L., George, C., Heard, D. E., Jackman, C. H., Kurylo, M. J., Mellouki, W., Orkin, V. L., Swartz, W. H., Wallington, T. J., Wine, P. H., and Burkholder, J. B.: The impact of current CH4 and N2O atmospheric loss process uncertainties on calculated ozone abundances and trends, J. Geophys. Res.: Atmos., 120, 5267–5293, https://doi.org/10.1002/2014jd022067, 2015.

Fu, Q. and Dong, C.: Global stratospheric methane loss from satellite observations, Proc. Natl. Acad. Sci., 123, e2529774123, https://doi.org/10.1073/pnas.2529774123, 2026.

https://doi.org/10.5194/egusphere-2026-2644
Preprint. Discussion started: 20 May 2026

Han, Y., Tian, W., Chipperfield, M. P., Zhang, J., Wang, F., Sang, W., Luo, J., Feng, W., Chrysanthou, A., and Tian, H.: Attribution of the Hemispheric Asymmetries in Trends of Stratospheric Trace Gases Inferred From Microwave Limb Sounder (MLS) Measurements, J. Geophys. Res.: Atmos., 124, 6283–6293, https://doi.org/10.1029/2018jd029723, 2019.

Mazière, M. D., Vigouroux, C., Bernath, P. F., Baron, P., Blumenstock, T., Boone, C., Brogniez, C., Catoire, V., Coffey, M., Duchatelet, P., Griffith, D., Hannigan, J., Kasai, Y., Kramer, I., Jones, N., Mahieu, E., Manney, G. L., Piccolo, C., Randall, C., Robert, C., Senten, C., Strong, K., Taylor, J., Tétard, C., Walker, K. A., and Wood, S.: Validation of ACE-FTS v2.2 methane profiles from the upper troposphere to the lower mesosphere, Atmos. Chem. Phys., 8, 2421–2435, https://doi.org/10.5194/acp-8-2421-2008, 2008.

Mote, P. W., Rosenlof, K. H., McIntyre, M. E., Carr, E. S., Gille, J. C., Holton, J. R., Kinnersley, J. S., Pumphrey, H. C., Russell, J. M., and Waters, J. W.: An atmospheric tape recorder: The imprint of tropical tropopause temperatures on stratospheric water vapor, J. Geophys. Res.: Atmos., 101, 3989–4006, https://doi.org/10.1029/95jd03422, 1996.

Pan, L. L., Honomichl, S. B., Kinnison, D. E., Abalos, M., Randel, W. J., Bergman, J. W., and Bian, J.: Transport of chemical tracers from the boundary layer to stratosphere associated with the dynamics of the Asian summer monsoon, J Geophys Res Atmospheres, 121, 14,159--14,174, https://doi.org/10.1002/2016jd025616, 2016.

Pan, L. L., Atlas, E. L., Honomichl, S. B., Smith, W. P., Kinnison, D. E., Solomon, S., Santee, M. L., Saiz-Lopez, A., Laube, J. C., Wang, B., Ueyama, R., Bresch, J. F., Hornbrook, R. S., Apel, E. C., Hills, A. J., Treadaway, V., Smith, K., Schauffler, S., Donnelly, S., Hendershot, R., Lueb, R., Campos, T., Viciani, S., D'Amato, F., Bianchini, G., Barucci, M., Podolske, J. R., Iraci, L. T., Gurganus, C., Bui, P., Dean-Day, J. M., Millán, L., Ryoo, J.-M., Barletta, B., Koo, J.-H., Kim, J., Liang, Q., Randel, W. J., Thornberry, T., and Newman, P. A.: East Asian summer monsoon delivers large abundances of very short-lived organic chlorine substances to the lower stratosphere, Proc. Natl. Acad. Sci., 121, e2318716121, https://doi.org/10.1073/pnas.2318716121, 2024.

Park, M., Randel, W. J., Kinnison, D. E., Garcia, R. R., and Choi, W.: Seasonal variation of methane, water vapor, and nitrogen oxides near the tropopause: Satellite observations and model simulations, J. Geophys. Res. Atmospheres, 109, 302–318, https://doi.org/10.1029/2003jd003706, 2004.

Park, M., Randel, W. J., Emmons, L. K., Bernath, P. F., Walker, K. A., and Boone, C. D.: Chemical isolation in the Asian monsoon anticyclone observed in Atmospheric Chemistry Experiment (ACE-FTS) data, Atmos. Chem. Phys., 8, 757--764, https://doi.org/10.5194/acp-8-757-2008, 2008.

Park, M., Randel, W. J., Emmons, L. K., and Livesey, N. J.: Transport pathways of carbon monoxide in the Asian summer monsoon diagnosed from Model of Ozone and Related Tracers (MOZART), J Geophys Res Atmospheres 1984 2012, 114, https://doi.org/10.1029/2008jd010621, 2009.

https://doi.org/10.5194/egusphere-2026-2644
Preprint. Discussion started: 20 May 2026

Patra, P. K., Houweling, S., Krol, M., Bousquet, P., Belikov, D., Bergmann, D., Bian, H., Cameron-Smith, P., Chipperfield, M. P., Corbin, K., Fortems-Cheiney, A., Fraser, A., Gloor, E., Hess, P., Ito, A., Kawa, S. R., Law, R. M., Loh, Z., Maksyutov, S., Meng, L., Palmer, P. I., Prinn, R. G., Rigby, M., Saito, R., and Wilson, C.: TransCom model simulations of CH4 and related species: linking transport, surface flux and chemical loss with CH4 variability in the troposphere and lower stratosphere, Atmos. Chem. Phys., 11, 12813–12837, https://doi.org/10.5194/acp-11-12813-2011, 2011.

Ploeger, F. and Garny, H.: Hemispheric asymmetries in recent changes in the stratospheric circulation, Atmos. Chem. Phys., 22, 5559–5576, https://doi.org/10.5194/acp-22-5559-2022, 2022.

Ploeger, F., Günther, G., Konopka, P., Fueglistaler, S., Müller, R., Hoppe, C., Kunz, A., Spang, R., Grooß, J. -U., and Riese, M.: Horizontal water vapor transport in the lower stratosphere from subtropics to high latitudes during boreal summer, J Geophys Res Atmospheres, 118, 8111--8127, https://doi.org/10.1002/jgrd.50636, 2013.

Ploeger, F., Konopka, P., Walker, K., and Riese, M.: Quantifying pollution transport from the Asian monsoon anticyclone into the lower stratosphere, Atmos Chem Phys, 17, 7055–7066, https://doi.org/10.5194/acp-17-7055-2017, 2017.

Prignon, M., Chabrillat, S., Friedrich, M., Smale, D., Strahan, S. E., Bernath, P. F., Chipperfield, M. P., Dhomse, S. S., Feng, W., Minganti, D., Servais, C., and Mahieu, E.: Stratospheric Fluorine as a Tracer of Circulation Changes: Comparison Between Infrared Remote-Sensing Observations and Simulations With Five Modern Reanalyses, J. Geophys. Res.: Atmos., 126, https://doi.org/10.1029/2021jd034995, 2021.

Randel, W. J. and Park, M.: Deep convective influence on the Asian summer monsoon anticyclone and associated tracer variability observed with Atmospheric Infrared Sounder (AIRS), J. Geophys. Res.: Atmos., 111, 314–327, https://doi.org/10.1029/2005jd006490, 2006.

Randel, W. J., Park, M., Emmons, L., Kinnison, D., Bernath, P., Walker, K. A., Boone, C., and Pumphrey, H.: Asian Monsoon Transport of Pollution to the Stratosphere, Science, 328, 611–613, https://doi.org/10.1126/science.1182274, 2010.

Randel, W. J., Moyer, E., Park, M., Jensen, E., Bernath, P., Walker, K., and Boone, C.: Global variations of HDO and HDO/H2O ratios in the upper troposphere and lower stratosphere derived from ACE-FTS satellite measurements, J. Geophys. Res.: Atmos., 117, 303–319, https://doi.org/10.1029/2011jd016632, 2012.

Riese, M., Ploeger, F., Rap, A., Vogel, B., Konopka, P., Dameris, M., and Forster, P.: Impact of uncertainties in atmospheric mixing on simulated UTLS composition and related radiative effects, J. Geophys. Res. Atmospheres, 117, 305–315, https://doi.org/10.1029/2012jd017751, 2012.

https://doi.org/10.5194/egusphere-2026-2644
Preprint. Discussion started: 20 May 2026

Riese, M., Hoor, P., Rolf, C., Kunkel, D., Vogel, B., Köllner, F., Pöhlker, M., Ploeger, F., Ungermann, J., Woiwode, W., Johansson, S., Bauer, R., Barmpounis, K., Borrmann, S., Brauner, P., Clemens, J., Dragoneas, A., Ekinci, F., Emig, N., Engel, A., Eppers, O., Fadnavis, S., Friedl-Vallon, F., Geldenhuys, M., Günther, G., Grooß, J. U., Hegglin, M. I., Höpfner, M., Jesswein, M., Joppe, P., Kaumanns, J., Kachula, O., Keber, T., Kretschmer, E., Lachnitt, H. C., Lauther, V., Lloyd, P. E., Molleker, S., Müller, R., Neubert, T., Ort, L., Pöschl, U., Pöhlker, C., Rapp, M., Retzlaff, M., Rhode, S., Schneider, J., Schuck, T., Sinnhuber, B.-M., Spelten, N., Strobel, J., Tomsche, L., Turhal, K., Luijt, R. van, Versick, S., Voigt, C., Volk, M., Hobe, M. von, Weyland, F., Zahn, A., Ziereis, H., and Zlotos, L. O.: Long-range transport of polluted Asian summer monsoon air to high latitudes during the PHILEAS campaign in the boreal summer 2023, Bull. Am. Meteorol. Soc., https://doi.org/10.1175/bams-d-24-0232.1, 2025.

Saunois, M., Martinez, A., Poulter, B., Zhang, Z., Raymond, P. A., Regnier, P., Canadell, J. G., Jackson, R. B., Patra, P. K., Bousquet, P., Ciais, P., Dlugokencky, E. J., Lan, X., Allen, G. H., Bastviken, D., Beerling, D. J., Belikov, D. A., Blake, D. R., Castaldi, S., Crippa, M., Deemer, B. R., Dennison, F., Etiope, G., Gedney, N., Höglund-Isaksson, L., Holgerson, M. A., Hopcroft, P. O., Hugelius, G., Ito, A., Jain, A. K., Janardanan, R., Johnson, M. S., Kleinen, T., Krummel, P. B., Lauerwald, R., Li, T., Liu, X., McDonald, K. C., Melton, J. R., Mühle, J., Müller, J., Murguia-Flores, F., Niwa, Y., Noce, S., Pan, S., Parker, R. J., Peng, C., Ramonet, M., Riley, W. J., Rocher-Ros, G., Rosentreter, J. A., Sasakawa, M., Segers, A., Smith, S. J., Stanley, E. H., Thanwerdas, J., Tian, H., Tsuruta, A., Tubiello, F. N., Weber, T. S., Werf, G. R. van der, Worthy, D. E. J., Xi, Y., Yoshida, Y., Zhang, W., Zheng, B., Zhu, Q., Zhu, Q., and Zhuang, Q.: Global Methane Budget 2000–2020, Earth Syst. Sci. Data, 17, 1873–1958, https://doi.org/10.5194/essd-17-1873-2025, 2025.

Schmidt, M., Bernath, P., Boone, C., Lecours, M., and Steffen, J.: Trends in atmospheric composition between 2004–2023 using version 5 ACE-FTS data, J. Quant. Spectrosc. Radiat. Transf., 325, 109088, https://doi.org/10.1016/j.jqsrt.2024.109088, 2024.

Strahan, S. E., Smale, D., Douglass, A. R., Blumenstock, T., Hannigan, J. W., Hase, F., Jones, N. B., Mahieu, E., Notholt, J., Oman, L. D., Ortega, I., Palm, M., Prignon, M., Robinson, J., Schneider, M., Sussmann, R., and Velazco, V. A.: Observed Hemispheric Asymmetry in Stratospheric Transport Trends From 1994 to 2018, Geophys. Res. Lett., 47, https://doi.org/10.1029/2020gl088567, 2020.

Vogel, B., Günther, G., Müller, R., Grooß, J.-U., Hoor, P., Krämer, M., Müller, S., Zahn, A., and Riese, M.: Fast transport from Southeast Asia boundary layer sources to northern Europe: rapid uplift in typhoons and eastward eddy shedding of the Asian monsoon anticyclone, Atmos. Chem. Phys., 14, 12745--12762, https://doi.org/10.5194/acp-14-12745-2014, 2014.

Vogel, B., M\"uller, R., G\"unther, G., Spang, R., Hanumanthu, S., Li, D., Riese, M., and Stiller, G. P.: Lagrangian simulations of the transport of young air masses to the top of the Asian monsoon anticyclone and into the tropical pipe, Atmos. Chem. Phys., 19, 6007--6034, https://doi.org/10.5194/acp-19-6007-2019, 2019.

https://doi.org/10.5194/egusphere-2026-2644
Preprint. Discussion started: 20 May 2026

Xiong, X., Houweling, S., Wei, J., Maddy, E., Sun, F., and Barnet, C.: Methane plume over south Asia during the monsoon season: satellite observation and model simulation, Atmos. Chem. Phys., 9, 783–794, https://doi.org/10.5194/acp-9-783-2009, 2009.

Yi, Y., Cai, Z., Liu, Y., Tao, M., Fang, S., Yang, D., Bai, Z., Liang, M., Yao, B., Bian, J., Honomichl, S. B., Randel, W. J., and Pan, L. L.: AirCore Observations at Northern Tibetan Plateau During the Asian Summer Monsoon, Geophys. Res. Lett., 51, 256–265, https://doi.org/10.1029/2024gl109256, 2024.

Yi, Y., Cai, Z., Liu, Y., Fang, S., Liang, M., Tao, M., Yang, D., Yao, B., Bai, Z., and Bian, J.: Observation of CH4, CO and N2O in the upper troposphere and lower stratosphere over the Qinghai–Tibet Plateau, Environ. Res. Lett., 21, 034009, https://doi.org/10.1088/1748-9326/ae34cd, 2026.

Yu, X., Millet, D. B., Henze, D. K., Turner, A. J., Delgado, A. L., Bloom, A. A., and Sheng, J.: A high-resolution satellite-based map of global methane emissions reveals missing wetland, fossil fuel, and monsoon sources, Atmos. Chem. Phys., 23, 3325–3346, https://doi.org/10.5194/acp-23-3325-2023, 2023.

Zeng, Z.-C., Byrne, B., Gong, F.-Y., He, Z., and Lei, L.: Correlation between paddy rice growth and satellite-observed methane column abundance does not imply causation, Nat. Commun., 12, 1163, https://doi.org/10.1038/s41467-021-21434-7, 2021.